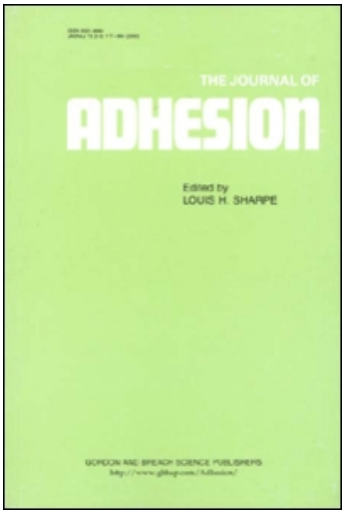

The Journal of Adhesion
Publication details, including instructions for authors and subscription information:
http://www.informaworld.com/smpp/title~content=t713453635

AN IMPROVED COMBINING RULE FOR SOLID-LIQUID ADHESION AND INTERMOLECULAR POTENTIALS: FORMULATION AND APPLICATION

Junfeng Zhang[a]; Daniel Y. Kwok[a]
[a] Nanoscale Technology and Engineering Laboratory, Edmonton, Alberta, Canada

Online publication date: 10 August 2010

To cite this Article Zhang, Junfeng and Kwok, Daniel Y.(2004) 'AN IMPROVED COMBINING RULE FOR SOLID-LIQUID ADHESION AND INTERMOLECULAR POTENTIALS: FORMULATION AND APPLICATION', The Journal of Adhesion, 80: 8, 745 — 765
To link to this Article: DOI: 10.1080/00218460490477693
URL: http://dx.doi.org/10.1080/00218460490477693

The Journal of Adhesion, 80: 745–765, 2004

ISSN: 0021-8464 print/1545-5823 online
DOI: 10.1080/00218460490477693

Taylor & Francis
Taylor & Francis Group

AN IMPROVED COMBINING RULE FOR SOLID–LIQUID ADHESION AND INTERMOLECULAR POTENTIALS: FORMULATION AND APPLICATION

Junfeng Zhang
Daniel Y. Kwok
Nanoscale Technology and Engineering Laboratory,
Department of Mechanical Engineering, University of Alberta,
Edmonton, Alberta, Canada

We have formulated a combining rule for solid–liquid adhesion and intermolecular potentials using macroscopic adhesion data. The combining rule is applied successfully to determine macroscopic solid–liquid adhesion and to calculate adhesion patterns using molecular theory. We found that the results determined from our combining rule are better than those by the 9:3, Steele's, and 12:6 combining rules in terms of scatters and details. Our results suggest that macroscopic data from careful contact angle and adhesion findings can be used to infer relationships of unlike solid–fluid interactions at a molecular level.

Keywords: Combining rule; Solid surface tensions; Adhesion; Contact angles; Intermolecular potential

INTRODUCTION

Interfacial free energy plays an important role in a variety of phenomena and processes such as wetting, spreading, and floatation. However, direct measurement of the solid–vapor (γ_{sv}) and solid–liquid (γ_{sl}) interfacial tensions is not available because of the absence of

Received 1 December 2003; in final form 13 April 2004.

One of a collection of papers honoring A. W. Newmann, the recipient in February 2004 of *The Adhesion Society Award for Excellence in Adhesion Science, Sponsored by 3M*.

This research was supported, in part, by the Alberta Ingenuity Establishment Fund, Canada Research Chair (CRC) Program, Canada Foundation for Innovation (CFI), and Natural Sciences and Engineering Research Council of Canada (NSERC). JZ acknowledges financial support from the Alberta Ingenuity Studentship Fund.

Address correspondence to Daniel Y. Kwok, Department of Mechanical Engineering, University of Alberta, Alberta, T6G 2G8, Canada. E-mail: daniel.y.kwok@ualberta.ca

solid mobility. Among the different indirect approaches in determining solid surface tensions, contact angle is believed to be the simplest, and hence it is the most widely used approach [1, 2].

The possibility of estimating solid surface tensions from contact angles relies on a relation known as Young's equation [3],

$$\gamma_{lv} \cos \theta_Y = \gamma_{sv} - \gamma_{sl}. \tag{1}$$

Here γ_{lv} is the liquid–vapor interfacial tension and θ_Y is the Young contact angle, *i.e.*, a contact angle that can be inserted into Young's equation. Within the context of this work, we assume the experimental contact angles, θ, to be the Young contact angle, θ_Y. Since Young's equation (Equation (1)) contains only two measurable quantities, γ_{lv} and θ, an additional expression relating γ_{sv} and γ_{sl} must be sought. Such an equation can be formulated using experimental adhesion or contact angle data.

The origin of surface tensions arises from the existence of unbalanced intermolecular forces among molecules at the interface. Recently, starting from macroscopic experimental adhesion patterns, Kwok and Neumann [4] proposed a fruitful procedure in formulating a new combining rule that is meant to better reflect solid–liquid interactions for intermolecular potentials. On the other hand, using a generalized van der Waals model and a mean-field approximation, van Giessen *et al.* [5] presented a calculation of surface tensions from intermolecular potentials, which is in fact similar to that of Sullivan [6]. Their calculated surface tensions of selected liquids were in reasonably good agreement with the measured data. However, the behavior of contact angles (the curve of $\cos\theta$ *versus* γ_{lv}) deviates considerably from the experimental trend. We noticed that no combining rule was involved in the calculations of the liquid–vapor surface tension (γ_{lv}); such a relation, however, was required for the calculations of γ_{sv} and γ_{sl} and, hence, $\cos\theta$, in order to evaluate the solid–fluid fluid intermolecular potential strength. Therefore, it is reasonable to attribute the discrepancy between the calculated and experimental $\cos\theta$ to the choice of the combining rule involved. By employing a better combining rule that represents more accurately the intermolecular attractions, we speculate that the calculation results of contact angles should be improved accordingly.

Recently, we have studied the most commonly used combining rules, and the one proposed by Kwok and Newmann. [4] using the method in Gissen *et al.* [5], and found that their behaviors are not satisfactory [7, 8]. In this article we propose a new formulation for solid–liquid adhesion using macroscopic adhesion data based on the original idea by Kwok and Newmann [4]. We will also examine the

application of the derived combining rule in molecular theory by calculating the solid–liquid adhesion patterns using a van der Waals model with a mean field approximation, similar to the previous work [5, 7, 8]. The calculated adhesion and contact angle patterns by the new combining rule are compared against those from the 9:3, Steele's, 12:6, and Kwok's combining rules. It will be shown that the newly formulated combining rule presented here follows the experimental patterns very closely.

THEORY

Combining Rules

In the study of mixtures and solid–liquid systems, combining rules are used to evaluate the interaction potential parameters between different molecules in terms of those between the same kind of molecules [6, 9–16]. In general, the minimum of the solid–liquid interaction potential, ϵ_{sl}, is often expressed in the following manner:

$$\epsilon_{sl} = g(\sigma_l/\sigma_s)\sqrt{\epsilon_{ss}\epsilon_{ll}}, \tag{2}$$

where $g(\sigma_l/\sigma_s)$ is a function of σ_l and σ_s; they are, respectively, the collision diameters for the liquid and solid molecules. Respectively ϵ_{ss} and ϵ_{ll} are the minima in the solid–solid and liquid–liquid potentials. Several forms for the function of $g(\sigma_l/\sigma_s)$ have been suggested and utilized.

Among these rules, the Berthelot rule [17],

$$\epsilon_{ij} = \sqrt{\epsilon_{ii}\epsilon_{jj}}, \tag{3}$$

is the simplest and most widely used approximation, but it does not provide a secure basis for the understanding of unlike-pair interactions. It has been demonstrated [18–20] that the Berthelot geometric mean combining rule generally overestimates the strength of the unlikepair interaction *i.e.,* the geometric mean value is too large an estimate. By comparing ϵ_{sl} with the minimum in the (9:3) Lennard-Jones potential, one obtains a combining rule as

$$\epsilon_{sl} = \frac{1}{8}\left(1+\frac{\sigma_l}{\sigma_s}\right)^3\sqrt{\epsilon_{ss}\epsilon_{ll}}. \tag{4}$$

Al alternative form,

$$\epsilon_{sl} = \frac{1}{4}\left(1+\frac{\sigma_l}{\sigma_s}\right)^2\sqrt{\epsilon_{ss}\epsilon_{ll}}, \tag{5}$$

has been investigated by Steele [21] and others [22]. For comparison purpose, we call Equation (5) the *Steele combining rule* in this article. Furthermore, from the (12:6) Lennard-Jones potential, a (12:6) combining rule can be obtained as follows [4]:

$$\epsilon_{sl} = \left[\frac{4\sigma_l/\sigma_s}{(1+\sigma_l/\sigma_s)^2}\right]^3 \sqrt{\epsilon_{ss}\epsilon_{ll}}. \tag{6}$$

In general, these functions are normalized such that $g(\sigma_l/\sigma_s) = 1$ when $\sigma_l = \sigma_s$; they revert to the Berthelot geometric mean combining rule (Equation (3)). Nevertheless, adequate representation of unlike solid–liquid interactions from like pairs is rare, and their validity for solid–liquid systems lacks experimental support.

On the other hand, Kwok and Neumann [4] recently proposed a novel approach of combining rule formulation from macroscopic experimental results, and a modified rule based on the (12:6) combining rule was obtained:

$$\epsilon_{sl} = \left[\frac{4\sigma_l/\sigma_s}{(1+\sigma_l/\sigma_s)^2}\right]^{\left(\alpha_k k/\sigma_s^3\right)^{2/s}} \sqrt{\epsilon_{ss}\epsilon_{ll}}, \tag{7}$$

where k is, in general, a constant that depends on the Boltzmann constant, and absolute and critical temperatures.

Calculation of Interfacial Tensions and Contact Angles

In order to examine the combining rules at a molecular level, we employ a mean-field approximation here to calculate numerically the three interfacial tensions from molecular interactions. In our simple van der Waals model, the fluid molecules are idealized as hard spheres interacting with each other through a potential $\phi_{ff}(r)$, where τ is a distance between two interacting molecules. A Carnahan-Starling model [5, 16, 23] is adopted as the hard sphere reference system. For a planar interface formed by a liquid and its vapor, each of which occupies a semi-infinite space—$z > 0$ and $z < 0$, respectively—the surface tension is given by [5–7]

$$\gamma_{lv} = \min_{\rho} \int_{-\infty}^{+\infty} dz \left\{ F[\rho(z)] + \frac{1}{2}\rho(z) \int_{-\infty}^{+\infty} dz' \bar{\phi}_{ff}(z'-z)[\rho(z'-z) - \rho(z)] \right\}. \tag{8}$$

Here the minimum is taken over all possible density profiles, $\rho(z)$; F is the excess free energy; and $\bar{\phi}_{ff}$ represents the interaction potential

that has been integrated over the whole $x'y'$ plane. For the solid–fluid (*i.e.*, a solid–liquid or a solid–vapor) interface, the solid is modeled as a semi-infinite impenetrable wall occupying the domain of $z < 0$ and exerting an attraction potential *V(z)* to the fluid molecule at a distance z from the solid surface. The interfacial tension of such an interface can be obtained from

$$\gamma_{sf} = \gamma_s + \min_{\rho} \int_0^{+\infty} dz\{F[\rho(z)] + \rho(z)V(z) + \frac{1}{2}\rho(z)\int_0^{+\infty} dz'\bar{\phi}_{ff}(z'-z)[\rho(z') - \rho(z)] - \frac{1}{2}\rho^2(z)\int_{-\infty}^{0} dz'\bar{\phi}_{ff}(z'-z)\Big\}, \quad (9)$$

where γ_s is the solid–vacuum surface tension, a constant that exists in the calculations of γ_{sv} and γ_{sl}. This constant (γ_s) will be canceled out in the calculations of the contact angles and adhesion work *via* Young's equation, Equation (1); it has no impact on the implication of our results since we are interested only in the difference between γ_{sv} and γ_{sl}. Considering a solid with molecules interacting with fluid molecules through a potential $\phi_{sf}(\tau)$, we easily obtain the intermolecular potential *V(z)* by integrating $\phi_{sf}(\tau)$ over the solid domain. We wish to point out that the above equations for γ_{lv} and γ_{sf} (Equations (8) and (9)) are identical to those reported in Giessen *et al.* [5], and Sullivan [6], although the forms of equations are different.

We believe that the integral terms

$$-\frac{1}{2}\rho^2(z)\int_{-\infty}^{0} dz'\bar{\phi}_{ff}(z'-z)$$

in Equation (9) and

$$-\rho(z)\int_{-\infty}^{0} dz'\bar{\phi}_{ff}(z'-z)$$

in Equation (10) in Giessen *et al.* [5] are missing. Without such integral terms, for the case of a fluid against a wall with $V(z) = 0$, $\rho(z) = \rho_f$ (the density of bulk fluid) would be the solution to the Euler-Lagrange equation (Equation (10)) there. Thus, we would not be finding the "drying" layer of vapor between the bulk liquid and the wall. In the expressions of all combining rules there, *i.e*, Equations (12)–(14) in Giessen *et al.* [5] and throughout that paper, all of the terms d_s/d_f should be corrected as d_f/d_s [6]. We have employed σ_f/σ_s here, rather than d_f/d_s.

To carry out the calculations of interfacial tensions, and hence the contact angles, a given interaction potential is required. Here we assume a (12:6) Lennard-Jones potential model and consider only the attraction part. It should be noted that the Lennard-Jones potential function requires knowledge of two parameters: the potential strength, ϵ, and the collision diameter, σ. The potential strength ϵ_{sf} for $\phi_{sf}(r)$ is obtained from the fluid, ϵ_{ff}, and solid, ϵ_{ss} potential strengths *via* a combining rule, such as that given by Equations (5) or (7).

As mentioned above, the calculation of liquid surface tension, γ_{lv}, requires two parameters, ϵ_{ff} and σ_f, which can be related to the critical temperature, T_c, and pressure, P_c, of the liquid in the following expressions for the Carnahan-Starling model [5, 16]

$$k_B T_c = 0.18016\alpha/\sigma_f^3,$$
$$P_c = 0.01611\alpha/\sigma_f^6, \tag{10}$$

where k_B is the Boltzmann constant and α is the van der Waals parameter given by

$$\alpha = -\frac{1}{2}\int \phi_{ff}(r)dr. \tag{11}$$

The densities of the liquid, ρ_l, and vapor, ρ_v, were obtained by requiring the liquid and vapor to be in coexistence at a given temperature, T [5, 16]. In our calculations, we have selected thirty liquids of different molecular structures and have assumed T = 21°C, $\sigma_s = 10$ Å, and $\rho_s = 10^{27}$ molecules/m^3 for the solid surface.

RESULTS AND DISCUSSION

Solid–Liquid Adhesion Patterns

Kwok *et al.* [1, 4, 24] have recently published experimental contact angle patterns for a large number of polar and nonpolar liquids on a variety of low-energy solid surfaces. These contact angles were believed to the most accurate sets that had been produced so far, which satisfy the underlying assumptions of all contact angle approaches to determine solid surface tensions. While these approaches are, logically and conceptually, mutually exclusive, nevertheless they share the following basic assumptions:

1. All approaches rely on the validity and applicability of Young's equation for surface energetics from experimental contact angles.

2. Pure liquids are always used; surfactant solutions or mixtures of liquids should not be used, since they would introduce complications due to preferential adsorption.
3. The values of γ_{lv} and γ_{sv} (and γ_{sl}) are assumed to be constant during the experiment, *i.e.*, there should be no physical/chemical interaction between the solid and the liquid.
4. The liquid surface tensions of the test liquids should be higher than the anticipated solid surface tension.
5. The values of γ_{sv} going from liquid to liquid are also assumed to be constant, *i.e.*, independent of the liquids used.

The contact angle studies by Kwok *et al.* [1, 4, 24] have shown the complexities of contact angle phenomena, which prevent use of measurements for surface energetic calculations, by means of low-rate dynamic contact angle measurements using an automated drop shape analysis. It was found that there were three apparent contact angle complexities that violated the basic assumptions made in the interpretation of contact angles for solid surface tensions:

1. Slip/stick of the three-phase contact line;
2. Contact angle increases/decreases as the drop front advances; and
3. Liquid surface tension changes as the drop front advances.

These contact angles should not be used for the determination of solid surface tensions. With respect to the first point, slip/stick of the three-phase contact line indicates that Young's equation is not applicable. Increase/decrease in the contact angle and change in the liquid surface tension as the drop front advances violate the expectation of no physical/chemical interaction. Therefore, when the experimental contact angles and liquid surface tensions are not constant, they should be disregarded. A recent contact angle study [25] on self-assembled monolayers has illustrated the more complicated phenomena. After eliminating the meaningless (nonconstant) data, experimental contact angles on a large number of polymer surfaces yield smooth curves of $\gamma_{lv}\cos\theta$ *versus* γ_{lv}, $\cos\theta$ *versus* γ_{lv}, and W_{sl} *versus* γ_{lv} for one and the same solid surface. The solid–liquid work of adhesion, W_{sl}, can be obtained from experimental contact angles and liquid surface tensions through Equation (20). Here we replot their results in Figure 1 and will compare them with our patterns calculated from intermolecular potentials. Figure 1a illustrates that for a given solid surface, say the FC722 surface (Fluorad fluorochemical coating, 3M, St. Paul, MN, USA), the experimental solid–liquid work of adhesion, W_{sl}, increases as γ_{lv} increases and up to a maximum W_{sl} value identified as W_{sl}^{*}. Further increase in

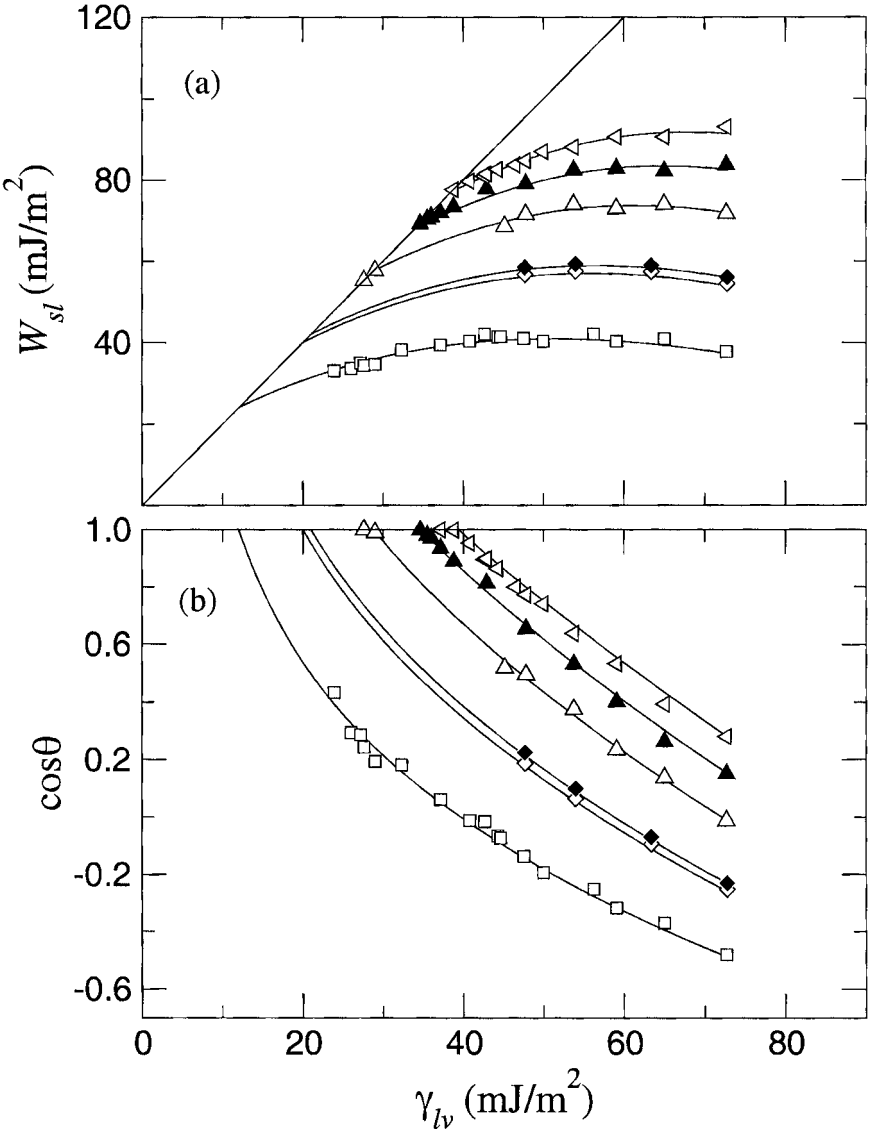

FIGURE 1 (a) The solid–liquid work of adhesion, W_{sl}, *versus* the liquid–vapor surface tension, γ_{lv}, and (b) cosine of the contact angle, $\cos\theta$, *versus* the liquid–vapor surface tension, γ_{lv}, for a fluorocarbon FC722 (□), hexatriacontane (◇), cholesteryl acetate (◆), poly(*n*-butyl methacrylate) (△), poly(methyl methacrylate/*n*-butyl methacrylate) (▲), and poly(methyl methacrylate) (◁) surfaces.

γ_{lv} causes W_{sl} to decrease from W_{sl}^*. The trend described here appears to shift systematically to the upper right for a more hydrophilic surface (such as PMMA) and to the lower left for a relatively more hydrophobic surface. There are also some indications that the location of the maximum point W_{sl}^* appears to shift to the right as surface hydrophobicity decreases. Figure 1b shows the experimental contact angle patterns in $\cos\theta$ *versus* γ_{lv}. We see that, for a given solid surface, as γ_{lv} decreases cosine of the contact angle ($\cos\theta$) increases, intercepting at $\cos\theta = 1$ with a "limiting" γ_{lv} value. We identify this 'limiting" value as γ_{lv}^c. As γ_{lv} decreases beyond this γ_{lv}^c value, contact angles become more or less zero ($\cos\theta \approx 1$), representing the case of complete wetting. The trend described here appears to change systematically to the right for a more hydrophilic surface (such as poly(methyl methacrylate): PMMA) and to the left for a relatively more hydrophobic surface (such as a fluorocarbon). Changing the solid surfaces in this manner changes the limiting γ_{lv}^c value, suggesting that γ_{lv}^c might be of indicative value as a solid property. In fact, Zisman labeled this γ_{lv}^c value as the critical surface tension of wetting of the solid surface γ_c.

Reformulation of a New Combining Rule

With careful examination of the modification procedures in Kwok and Neumann [4], we found that the assumption of $\gamma \propto \sigma^{-3}$ can be better represented by a more reasonable one: $\gamma \propto \sigma^{-2}$ [6]. Since surface tension is defined as the work required to generate a unit surface area, the relationship $\gamma \propto \sigma^{-2}$ is entirely compatible with this stipulation, as σ can be related directly to the changes in interfacial area. Therefore, we reformulate a new combining rule here and fit the expression to the experimental adhesion patterns.

According to the thermodynamic definition of the energy of adhesion, W_{sl}, and cohesion, W_{ss} and W_{ll} [26, 27], we have the following relations:

$$W_{sl} = \gamma_{lv} + \gamma_{sv} - \gamma_{sl}, \tag{12}$$

$$W_{ss} = 2\gamma_{sv}, \quad W_{ll} = 2\gamma_{lv}. \tag{13}$$

Because the free energy is directly proportional to the energy parameter [20, 27], *i.e.*, $W \propto \epsilon$, the general form of combining rule (Equation (2)) can be expressed as [17, 20, 27, 28]

$$W_{sl} = g(\sigma_l/\sigma_s)\sqrt{W_{ss}W_{ll}} = 2g(\sigma_l/\sigma_s)\sqrt{\gamma_{sv}\gamma_{lv}}. \tag{14}$$

Due to the relation of $\gamma \propto \sigma^{-2}$ [6], the function g can be further rewritten in terms of γ_{sv} and γ_{lv} explicitly:

$$g(\sigma_l/\sigma_s) = g\left(\gamma_{sv}^{1/2}/\gamma_{lv}^{1/2}\right). \tag{15}$$

Combining Equations (14) and (15) with Equations (3)–(6) yields, respectively, the following expressions:

$$W_{sl} = 2\sqrt{\gamma_{lv}\gamma_{sv}}, \tag{16}$$

$$W_{sl} = \frac{1}{4}\left[1 + \left(\frac{\gamma_{sv}}{\gamma_{lv}}\right)^{1/2}\right]^3 \sqrt{\gamma_{lv}\gamma_{sv}}, \tag{17}$$

$$W_{sl} = \frac{1}{2}\left[1 + \left(\frac{\gamma_{sv}}{\gamma_{lv}}\right)^{1/2}\right]^2 \sqrt{\gamma_{lv}\gamma_{sv}}, \tag{18}$$

and

$$W_{sl} = 2\left\{\frac{4(\gamma_{sv}/\gamma_{lv})^{1/2}}{\left[1 + (\gamma_{sv}/\gamma_{lv})^{1/2}\right]^2}\right\}^3 \sqrt{\gamma_{lv}\gamma_{sv}}. \tag{19}$$

Since W_{sl} now relates explicitly to γ_{lv} and γ_{sv}, the effect of changing γ_{lv} on W_{sl} can be examined for constant γ_{sv}.

Experimentally, one can in principle obtain the free energy of adhesion, W_{sl}, *via* contact angles through Young's equation (Equation (1)). Combining Equation (1) with the definition of W_{sl}, Equation (12) yields a relation of W_{sl} as a function of γ_{lv} and θ:

$$W_{sl} = \gamma_{lv}(1 + \cos\theta). \tag{20}$$

Thus, experimental results can be compared with those predicted from Equations (16)–(19); *i.e.*, contact angles of different liquids on one and the same solid surface can be employed to study the systematic effect of changing γ_{lv} on W_{sl} through θ.

Figure 2 displays the free energy of adhesion, W_{sl}, *versus* the liquid–vapor surface tension, γ_{lv}, from recent experimental contact angles for polystyrene (PS) [29], poly (styrene/methyl methacrylate, 70/30) P(S/MMA, 70/30) [30], and PMMA [31]; Equation (20) was used to relate θ to W_{sl}. The predicted patterns from Equations (16)–(19) for a hypothetical solid surface with $\gamma_{sv} = 30$ mJ/m^2 are also given in solid lines. These results suggest that the above combining rules do not

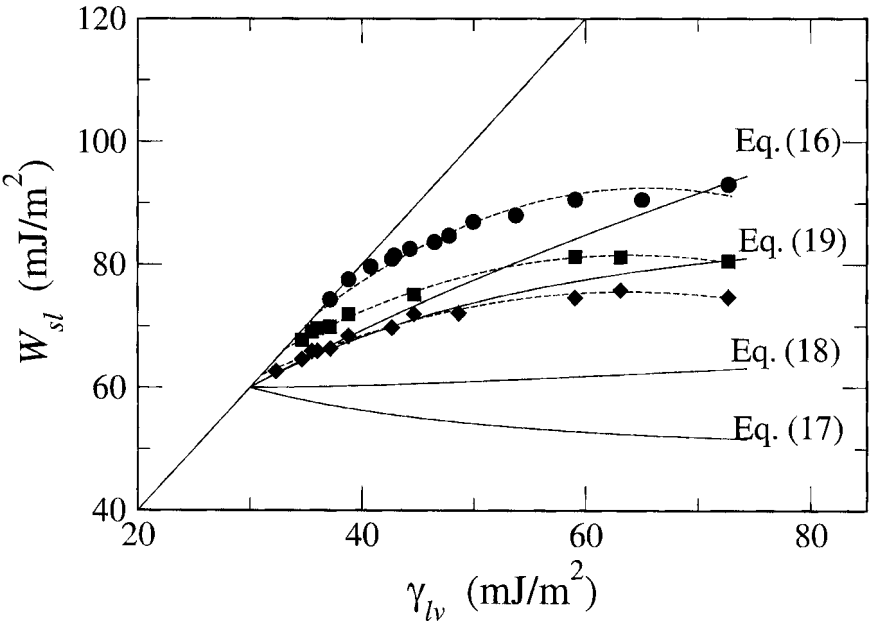

FIGURE 2 The free energy of adhesion, W_{sl}, *versus* γ_{lv} for polystyrene (PS) (circles), poly(styrene/methyl methacrylate, 70/30) P(S/MMA, 70/30) (squares), and poly(methyl methacrylate) PMMA (diamonds). The diagonal lines is the line of zero contact angle, *i.e.*, $W_{sl} = 2\gamma_{lv}$; other solid lines are the W_{sl} values predicted by Equations (16)–(19) using $\gamma_{sv} = 30\,\mathrm{mJ/m^2}$.

predict the observed adhesion patterns adequately. The (9:3) combining rule of Equation (17) even shows a monotonous decreasing fashion of W_{st} as γ_{lv} increases, which is clearly different from the experimental trends.

Nevertheless, closer scrutiny suggests that the form of the (12:6) combining rule in Equation (19) may be useful in predicting the experimental adhesion patterns. As a step toward such an investigation, we rewrite this equation in the following generalized form:

$$W_{sl} = 2\left\{\frac{4(\gamma_{sv}/\gamma_{lv})^{1/2}}{\left[1+(\gamma_{sv}/\gamma_{lv})^{1/2}\right]^2}\right\}^n \sqrt{\gamma_{lv}\gamma_{sv}}, \tag{21}$$

where n is a constant to be determined. For $n = 3$, Equation (21) reverts to Equation (19). The question now becomes how well this equation fits the experimental data in Figure 2. Assuming γ_{sv} to be constant for one and the same solid surface, experimental contact

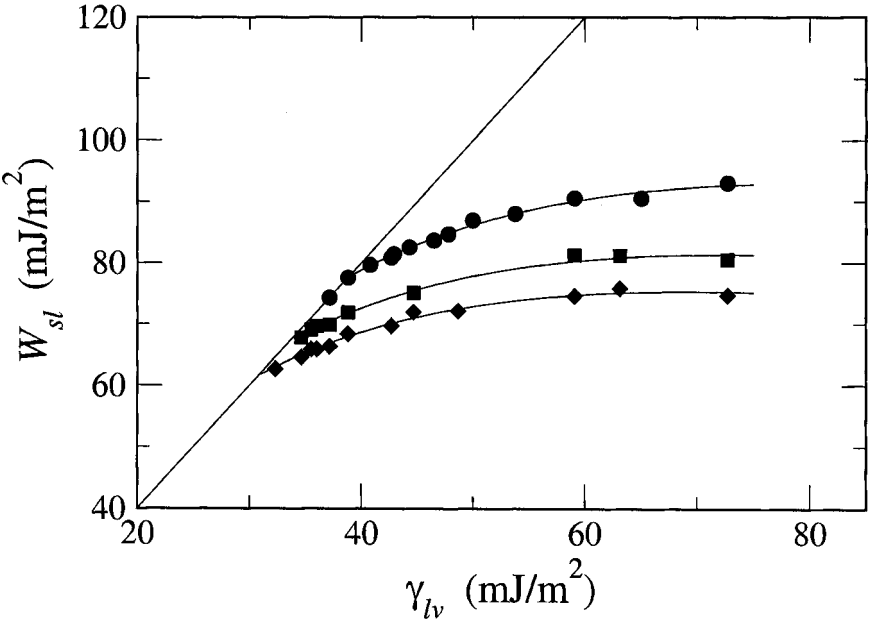

FIGURE 3 The fitted free energy of adhesion, W_{sl}, *versus* γ_{lv} for Equation (21), for the data in Figure 2: polystyrene (PS), poly(styrene/methyl methacrylate 70/30) P(S/MMA, 70/30), and poly(methyl methacrylate) PMMA.

angle data can be used to fit this equation using a least-squares scheme.

The best fits of Equation (21) to experimental data are shown in Figure 3. Clearly, Equation (21) provides a good fit to the experimental data, with the fitting results summarized in the second and third columns in Table 1. Although Equation (21) appears to fit the data well, there is some indication that the power term, n, is changing with

TABLE 1 Fitting Results of Experimental Energy of Adhesion from Contact Angles for Equation (21)

Solid surface	n	γ_{sv}	γ_{sv}/n	γ_{sv}/n^2
poly(methyl methacrylate), PMMA	5.61	38.85	6.925	1.234
poly(styrene/methyl methacrylate, 70/30), P(S/MMA, 70/30)	5.26	33.59	6.386	1.214
polystyrene, PS	4.98	30.74	6.173	1.239

γ_{sv} is expressed in mJ/m^2.

the solid surface. We noticed that n decreases systematically with solid surface tension, γ_{sv}. In Table 1, we attempted to normalized such changes by expressing the fitted results as γ_{sv}/n and γ_{sv}/n^2 in the fourth and fifth columns, respectively. We found that the values of γ_{sv}/n^2 appear to be essentially independent of the solid surfaces used. Averaging and weighting γ_{sv}/n^2 over the number of data used yields $\gamma_{sv}/n^2 = 1.23$ m^2/mJ. The relationship between the energy of adhesion, W_{sl}, and surface tensions, γ_{sv} and γ_{lv}, can now be expressed as

$$W_{sl} = 2\left\{\frac{4(\gamma_{sv}/\gamma_{lv})^{1/2}}{\left[1+(\gamma_{sv}/\gamma_{lv})^{1/2}\right]^2}\right\}^{(\tau\gamma_{sv})^{1/2}} \sqrt{\gamma_{lv}\gamma_{sv}}, \tag{22}$$

where $\tau = 1/1.23$ m^2/mJ $= 0.813$ m^2/mJ.

Predictive Power

Theoretically, combining Equations (22) with (20) allows determination of the solid surface tension, γ_{sv}, from a single pair of experimental data (γ_{lv}, θ) on a surface. Nevertheless, we fit Equation (22) to the experimental W_{sl} *versus* γ_{lv} values on one and the same solid surface to obtain the solid surface tension, γ_{sv}. Combining Equation (22) with Equation (20) yields

$$\cos\theta = -1 + 2\sqrt{\frac{\gamma_{sv}}{\gamma_{lv}}}\left\{\frac{4(\gamma_{sv}/\gamma_{lv})^{1/2}}{\left[1+(\gamma_{sv}/\gamma_{lv})^{1/2}\right]^2}\right\}^{(\tau\gamma_{sv})^{1/2}} \tag{23}$$

With a calculated γ_{sv} value, one can predict the contact angle from the liquid surface tension, γ_{lv}, by the above equation. To illustrate the prediction of Equations (22) and (23), we selected 5 other surfaces which were not used in the determination of the τ value here. The 5 surface are FC722 coated-fluorocarbons [32], Teflon® (FEP) [33], poly (*n*-butyl methacrylate) (P*n*BMA) [24, 34], poly(ethyl methacrylate) (PEMA) [24, 35], and poly(propene-*alt*-*N*-(*n*-propyl)maleimide) P (PPMI) [24, 36, 37]. The determined solid surface tensions, γ_{sv}, are listed in Table 2. It is apparent that the prediction of the γ_{sv} values agree well with the intuition that a fluorocarbon should have a γ_{sv} around 12–15 mJ/m^2 and the γ_{sv} for an ethyl methacrylate polymer (PEMA) should be less than that of the PMMA and should fall between 30–35 mJ/m^2. The averaged γ_{sv} values determined from

TABLE 2 Solid Surface Tension Values, γ_{sv}, Obtained from Equation (23) with $\tau = 0.813\ m^2/mJ$

	$\gamma_{sv}(mJ/m^2)$	
Solid surface	Equation (23)	Equation of state approach
FC722	14.9	12.1
FEP	19.7	17.8
P*n*BMA	30.0	28.8
PEMA	33.9	34.0
P(PPMI)	38.9	37.3

The averaged γ_{sv} values [4] determined from the equation of state approach from the same set of data are also given.

the equation of state approach using the same sets of experimental data are also given in Table 2 for comparison purposes. It can be seen that the γ_{sv} values obtained from Equation (23) are essentially identical to those determined from the equation of state approach.

Figure 4 displays the predicted and experimental adhesion, W_{sl}, and the cosine of the contact angle, $\cos\theta$, patterns for the 5 surfaces in Table 2. It is clear from Figure 4 that the predicted curves fit very well to the experimental data of W_{sl} and $\cos\theta$ *versus* γ_{lv}. It should be noted that these predicted values were calculated with $\tau = 0.813\ m^2/mJ$, which was obtained from the other three solid surfaces (PS, P(S/MMA, 70/30), and PMMA) as described earlier, Furthermore, the agreement between the two cases appears to be even more striking when a contact angle error of $\pm$ 1–2 degrees is considered.

Application in Molecular Theory

We have recently examine the combining rules discussed above in the section "Combining Rules" [7, 8]. For the completeness and convenience of comparison, we represented the results here in Figure 5. Thirty polar and non polar liquids have been used to calculate the interfacial tensions for the adhesion patterns using Berthelot's (9:3), Steele's, (12:6), and Kwok's combining rules [7, 8]. In order to change the hydrophilicity of the model surface and observe the change in patterns, we hypothesize that solid surface energy increases with stronger solid–solid interaction energy, ϵ_{ss}: increasing the solid–solid solid interactions increases the surface free energy required to generate a unit interfacial surface area. Thus, we increased the solid–solid

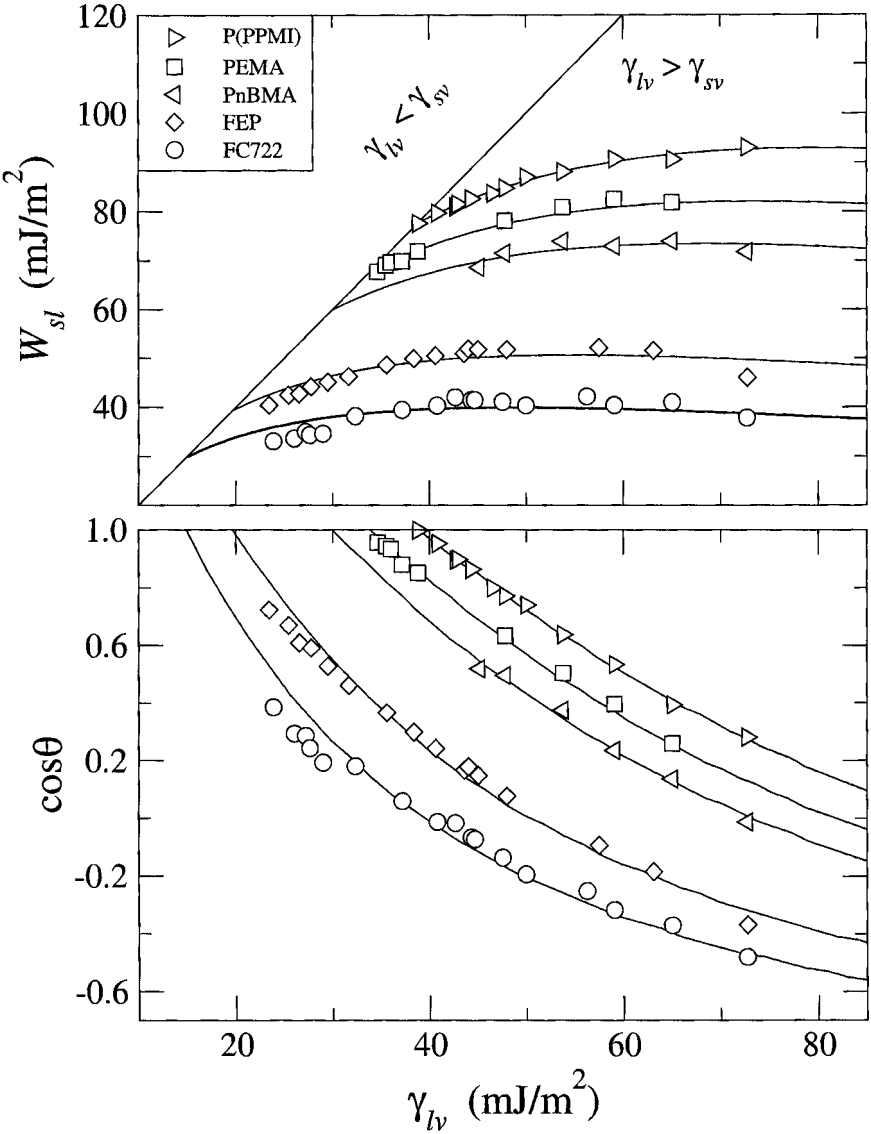

FIGURE 4 The predicted free energy of adhesion, W_{sl}, and cosine of contact angles, $\cos\theta$, *versus* γ_{lv} with $\tau = 0.813$ m^2/mJ for FC722 fluorocarban-coated surface (◯), Teflon (FEP) (◇), poly(*n*-butyl methacrylate) (P*n*BMA) (◁), poly (ethyl methacrylate) (PEMA) (□), and poly(propene-*alt*-*N*-(*n*-propyl) maleimide) P(PPMI) (▷).

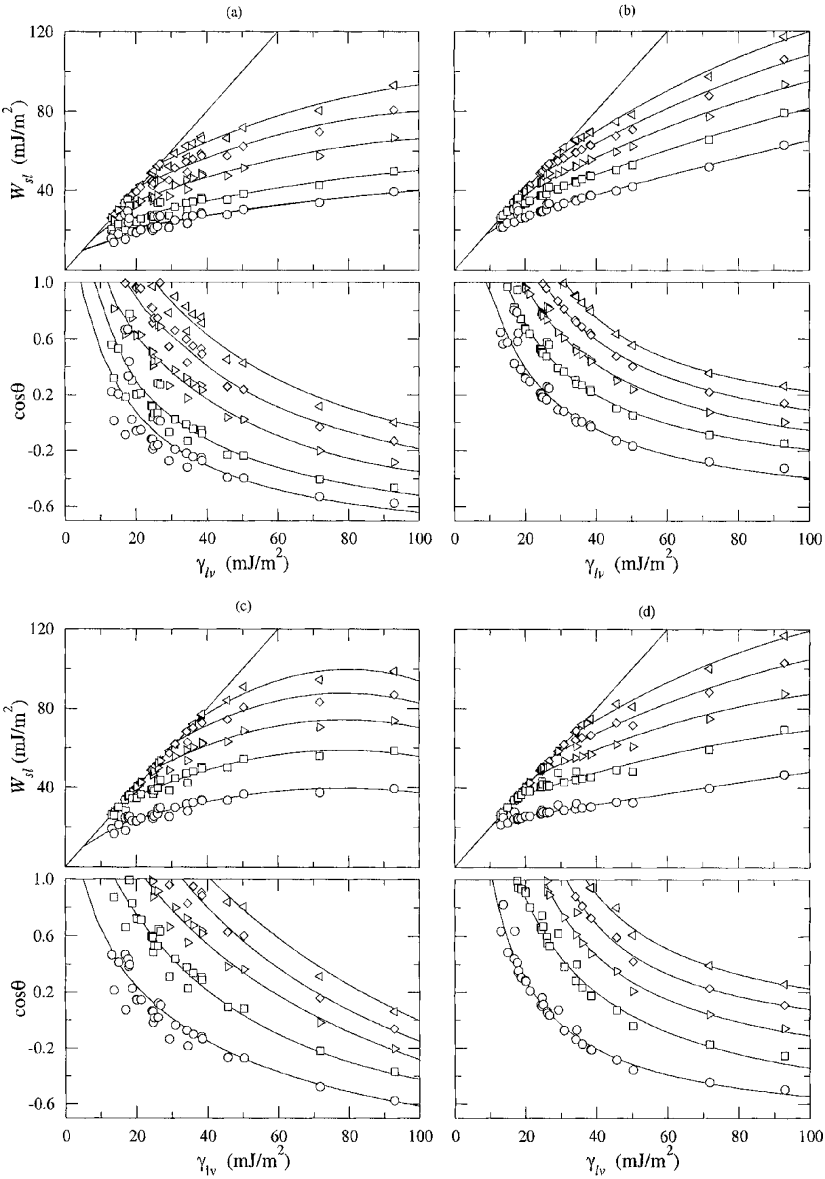

FIGURE 5 The solid–liquid work of adhesion, W_{sl}, *versus* the liquid–vapor surface tension, γ_{lv}, and cosine of the contact angle, $\cos\theta$, *versus* the liquid–vapor surface tension, γ_{lv}, calculated from (a) (9:3) combining rule, (b) Steele's combining rule, (c) (12:6) combining rule, and (d) Kwok's combining rule. The symbols are calculated data and the curves are the general trends of the data points.

interactions systematically to model hydrophilic surfaces and decreased the interactions for hydrophobic ones.

Our calculation results suggest that Berthelot's rule (Equation (3)) is the worst among all combining rules that we have considered, and the results are therefore not shown in Figure 5. With the exception of Berthelot's rule, the (9:3) rule (Equation (4)), Steele's rule (Equation (5)), the (12:6) rule (Equation (6)), and Kwok's rule (Equation (7)) all yield the general adhesion and contact angle patterns observed experimentally, but with larger scatters or less details [7, 8]. Kwok's rule (Equation (7)) produced the most similar behavior to the experimental results, but still with some scatters.

To apply the newly obtained rule here to the interfacial tension calculation, a relation of the potential parameters is needed. Since $W \propto \epsilon$ and $\gamma_{sv} \approx \mathrm{K}/\sigma_s^2$, Equation (22) can be rewritten as

$$\epsilon_{sl} = \left[\frac{4\sigma_l/\sigma_s}{(1+\sigma_l/\sigma_s)^2}\right]^{(\tau K/\sigma_s^2)^{1/2}} \sqrt{\epsilon_{ss}\epsilon_{ll}}. \tag{24}$$

Application of this combining rule requires knowledge of the unknown constant, K, which relates solid surface tension to molecular collision diameters. Since K is not readily known, we adopted here the assumption of $K \approx \gamma_{sv}\sigma_s^2 \approx \gamma_{lv}\sigma_l^2$ and, hence, $K/\sigma_S^2 \approx \gamma_{lv}\sigma_l^2/\sigma_s^2$, leading to

$$\epsilon_{sl} = \left[\frac{4\sigma_l/\sigma_s}{(1+\sigma_l/\sigma_s)^2}\right]^{(\tau\eta_v\sigma_l^2/\sigma_s^2)^{1/2}} \sqrt{\epsilon_{ss}\epsilon_{ll}}. \tag{25}$$

Using the theory and procedures described earlier, Equation (25) was used to evaluate the intermolecular potential strength, ϵ_{sl}, between the solid and fluid molecules. The calculated adhesion patterns are plotted in Figure 6. It can be seen that the newly formulated combining rule here (Equation (25)) generates a much steeper trend of the $\cos\theta$ *versus* γ_{lv} curve similar to the experimental trend observed. Other than providing a steeper trend, Equation (25) proposed here also generates much smoother curves of W_{sl} and $\cos\theta$ *versus* γ_{lv} than all other combining rules considered here. To elucidate this point, we superimposed the results generated from Equation (25) onto Figure 5 from Giessen *et al.* [5], and show them here in Figure 7. Here the solid intermolecular potential strength for Equation (25) was adjusted to produce a curve with $\gamma_c = 18$ mJ/m^2 on order to be compared with the data for a FEP surface. It can be seen in this figure that for low

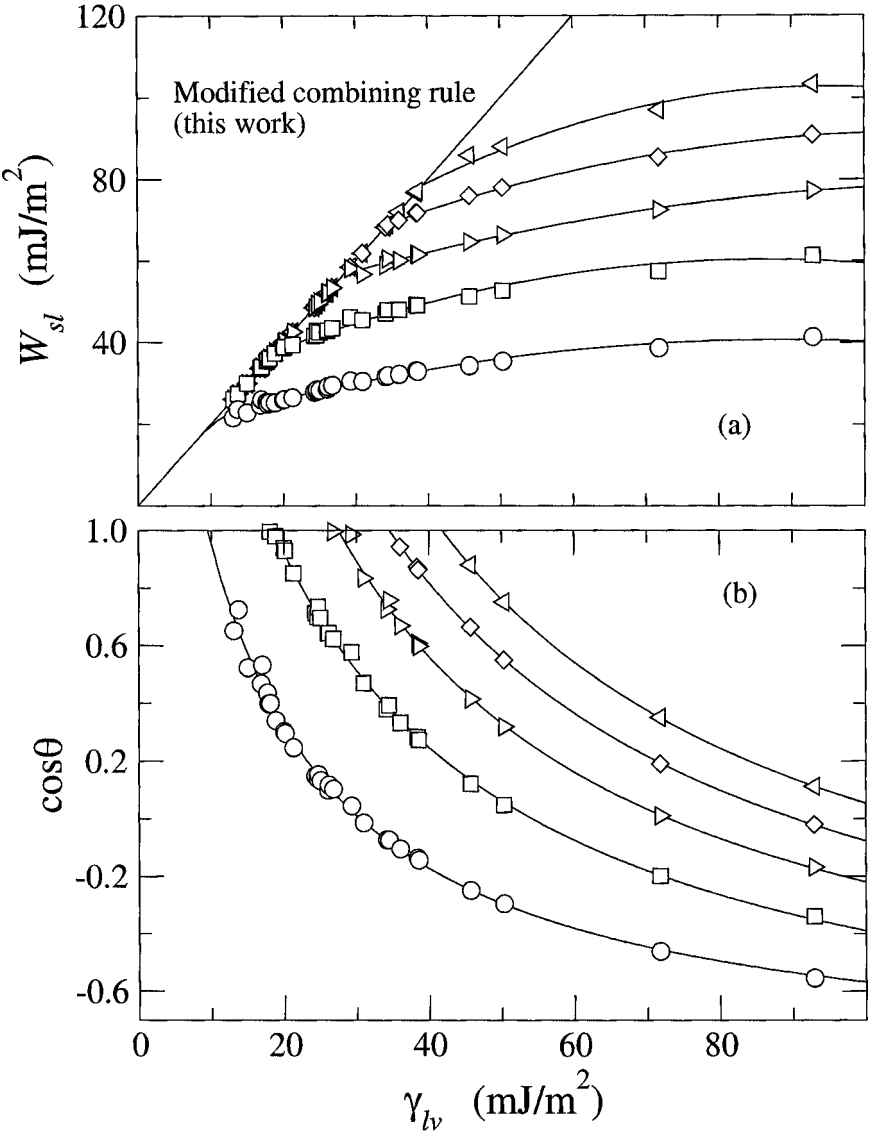

FIGURE 6 (a) The solid–liquid work of adhesion, W_{sl}, *versus* the liquid–vapor surface tension, γ_{lv}, and (b) cosine of the contact angle, $\cos\theta$, *versus* the liquid–vapor surface tension, γ_{lv}, calculated from the combining rule in Equation (25).

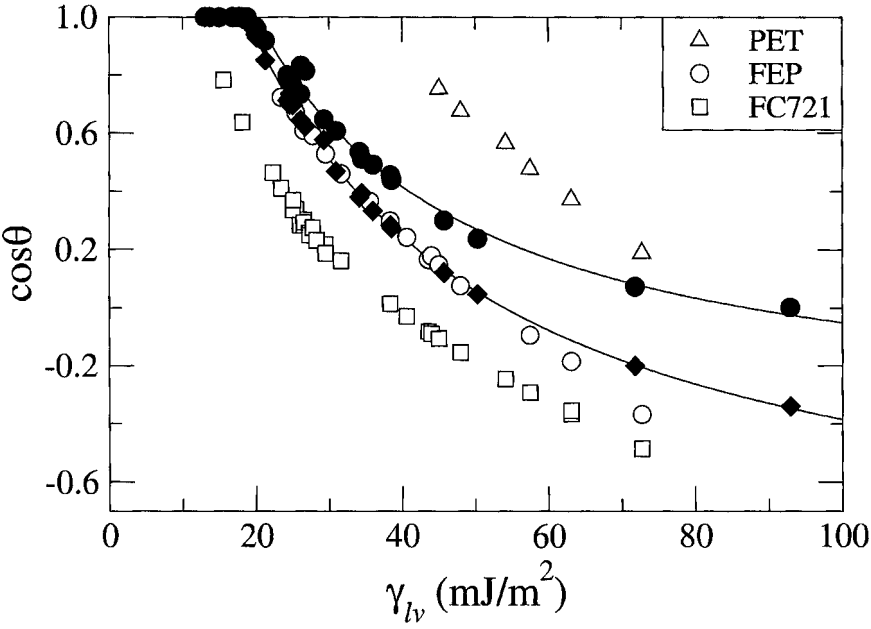

FIGURE 7 Cosine of the contact angle, $\cos\theta$, *versus* the liquid–vapor surface tension, γ_{lv}; open symbols are experimental data; (●) and (◆) represent the calculated data from Equations (5) and (25), respectively.

energy liquids ($\gamma_{lv} < 50\,\text{mJ/m}^2$) the calculated curve from Equation (25) follows the experimental points almost exactly. Because of the existence of hydrogen bonding in the high-energy liquids such as hydrazine and water, which are not considered in our theoretical model, these calculated W_{sl} and $\cos\theta$ tend to deviate from the experimental results. Nevertheless, if we compare the absolute values of $\cos\theta$ between the calculated and experimental results for water and hydrazine, the results would be very similar: for example, the calculated $\cos\theta$ of water on the FEP is -0.34, while the experimental value is -0.37. If we plot Figure 6 using the experimental surface tension of water and hydrazine as 72.8 and 67.6 mJ/m^2 rather than the calculated ones as 92.3 and 71.8 mJ/m^2, respectively, our calculated curve would fall exactly on the experimental data of FEP. According to the above analysis, it is more apparent that the calculated data from our modified-rule Equation (25) follows the experimental results very closely. Superposition of the calculated results onto the experimental patterns in Figure 8 illustrates the similarity of the two patterns more clearly (FC721, noted in the inset in

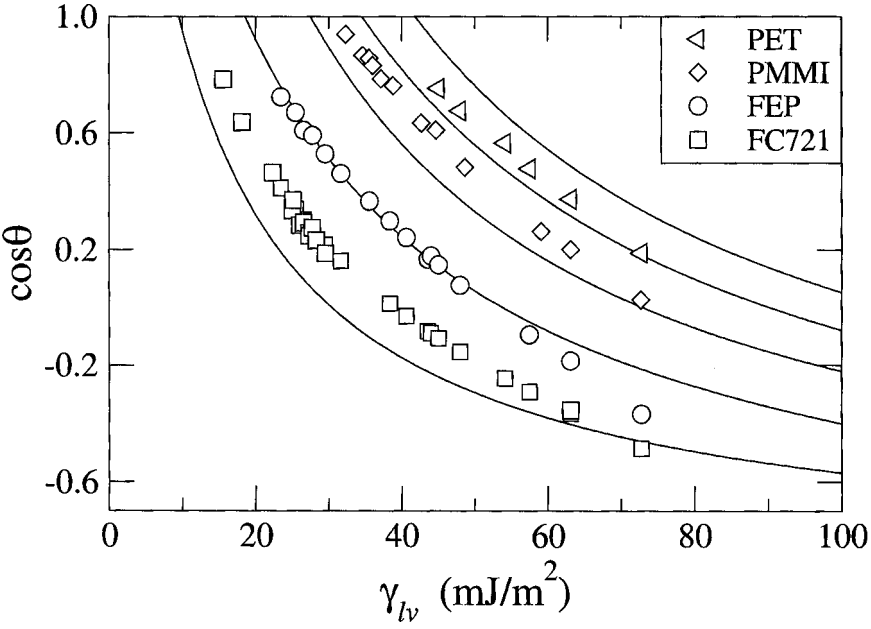

FIGURE 8 Superposition of experimental and calculated cosine of the contact angles, $\cos\theta$, *versus* the liquid–vapor surface tension, γ_{lv}; experimental data and calculated curves are represented by open symbols and solid lines, respectively.

Figures 7 and 8 refer to a Fluorad® fluorochemical coating, similar to FC722, from 3M, St. Paul, MN, USA).

SUMMARY

We have formulated a new combining rule between γ_{lv} and γ_{sv} for W_{sl} from experimental adhesion patterns. The obtained relation gives a good fit to experimental adhesion and contact angle data for the systems studied. By extending such a relation to the molecular level, we have derived an improved combining rule for intermolecular potentials and employed a van der Waals model using a mean field approximation for calculation of the adhesion and contact angle patterns. The calculated patterns follow the experimental results almost exactly. The remarkable agreement between the predicted and experimental data, both at a macroscopic and molecular level, suggests that the combining rule we derived here is useful to represent the relationship for solid–liquid adhesion as well as solid–fluid intermolecular potentials.

REFERENCES

[1] Kwok, D. Y. and Neumann, A. W., *Adv. Colloid Interface Sci.* **81**, 167–249 (1999).
[2] Sharma, P. K. and Rao, K. H., *Adv. Colloid Interface Sci.* **98**, 341–463 (2002).
[3] Young, T., *Philos. Trans. R. Soc. London* **95**, 65–87 (1805).
[4] Kwok, D. Y. and Neumann, A. W., *J. Phys. Chem. B* **104**(4), 741–746 (2000).
[5] Giessen, A. E., Bukman, D. J., and Widom, B., *J. Colloid Interface Sci.* **192**, 257–265 (1997).
[6] Sullivan, D. E., *J. Chem. Phys.* **74**(4), 2604–2615 (1981).
[7] Zhang, J. and Kwok, D. Y., *J. Phys. Chem. B.* **106**, 12594–12599 (2002).
[8] Zhang, J. and Kwok. D. Y., *Langmuir* **19**, 4666–4672 (2003).
[9] Chao, K. C. and Robinson, J. R. L., *Equation of State: Theories and Applications* (ACS Washington, DC, 1986).
[10] Fender, B. E. F. and Halsey, Jr., G. D., *J. Chem. Phys.* **36**. 1881–1888 (1962).
[11] Hudson, G. H. and McCoubrey, J. C., *Trans. Faraday Soc.* **56**, 761–766 (1960).
[12] Matyushov, D. V. and Schmid, R., *J. Chem. Phys.* **104**(21), 8627–8638 (1996).
[13] Reed, T. M., *J. Phys. Chem.* **59**, 425–428 (1955).
[14] Rowlinson, J. S. and Swinton, F. L., *Liquids and Liquid Mixtures* (Butterworth Scientific, London, 1981).
[15] Steele, W. A., *The Interaction of Gases with Solid Surfaces* (Pergamon Press, New York, 1974).
[16] Sullivan, D. E., *Phys. Rev. B* **20**(10), 3991–4000 (1979).
[17] Berthelot, D., *Compt. Rend.* **126**(1703), 1857 (1898).
[18] Israelachvili, J. N., *Proc. R. Soc. London A* **331**, 39–55 (1972).
[19] Kestin, J. and Mason, E. A., *AIP Conf. Proc.* **11**, 137–192 (1973).
[20] Maitland, G. C., Rigby, M., Smith, E. B., and Wakeham, W. A., *Intermolecular Forces: Their Origin and Determination* (Clarendon Press, Oxford, 1981).
[21] Steele, W. A., *Surf. Sci.* **36**, 317–352 (1973).
[22] Lane, J. E. and Spurling, T. H., *Aust. J. Chem.* **29**, 2103–2121 (1976).
[23] Carnahan, N. F. and Starling, K. E., *Phys. Rev. A* **1**(6), 1672–1673 (1970).
[24] Kwok, D. Y., Ng, H., and Neumann, A. W., *J. Colloid Interface Sci.* **225**(2), 323–328 (2000).
[25] Yang, J., Han, J., Isaacson, K., and Kwok, D. Y., *Langmuir* **19**, 9231–9238 (2003).
[26] Dupré, A., *Théorie Mécanique de la Chaleur* (Gauthier-Villars, Paris, 1969).
[27] Good, R. J. and Elbing, E., *Ind. Eng. Chem.* **62**(3), 72–96 (1970).
[28] Girifalco, L. A. and Good, R. J., *J. Phys. Chem.* **61**, 904–909 (1957).
[29] Kwok, D. Y., Lam, C. N. C., Li, A., Zhu, K., Wu, R., and Neuman, A. W., *Polym. Eng. Sci.* **38**, 1675–1684 (1998).
[30] Kwok, D. Y., Lam, C. N. C., and Neumann, A. W., *Colloid J.* **62**(3), 324–335 (2000).
[31] Kwok, D. Y., Leung, A., Lam, C. N. C., Li, A., Wu, R., and Neumann, A. W., *J Colloid Interface Sci.* **206**, 44–51 (1998).
[32] Kwok, D. Y., Lin, R., Mui, M., and Neumann, A. W., *Colloids Surfaces A: Physicochem. Eng. Aspects* **116**, 63–77 (1996).
[33] Li, D. and Neumann, A. W., *J. Colloid Interface Sci.* **148**, 190–200 (1992).
[34] Kwok, D. Y., Leung, A., Li, A., Lam, C. N. C., Wu, R., and Neumann, A. W., *Colloid Polym. Sci.* **276**, 459–469 (1998).
[35] Kwok, D. Y., Wu, R., Li, A., and Neumann, A. W., *J. Adhesion Sci. Tech.* **14**(5), 719–743 (2000).
[36] Kwok, D. Y., Gietzelt, T., Grundke, K., Jacobasch, H.-J., and Neumann, A. W., *Langmuir* **13**, 2880–2894 (1997).
[37] Kwok, D. Y., Lam, C. N. C., Li, A., Leung, A., and Neumann, A. W., *Langmuir* **14**, 2221–2224 (1998).